Interaction between depolarization effects, interface layer, and fatigue behavior in PZT thin film capacitors

U. Böttger, and R. Waser

Citation: Journal of Applied Physics **122**, 024105 (2017); doi: 10.1063/1.4992812
View online: http://dx.doi.org/10.1063/1.4992812
View Table of Contents: http://aip.scitation.org/toc/jap/122/2
Published by the American Institute of Physics

Interaction between depolarization effects, interface layer, and fatigue behavior in PZT thin film capacitors

U. Böttger[1,a] and R. Waser[1,2]
[1]*Institut für Werkstoffe der Elektrotechnik 2, RWTH Aachen University, 52056 Aachen, Germany*
[2]*Peter-Grünberg-Institut 7, Forschungszentrum Jülich GmbH, 52425 Jülich, Germany*

(Received 3 February 2017; accepted 26 June 2017; published online 13 July 2017)

The existence of non-ferroelectric regions in ferroelectric thin films evokes depolarization effects leading to a tilt of the $P(E)$ hysteresis loop. The analysis of measured hysteresis of lead zirconate titanate (PZT) thin films is used to determine a depolarization factor which contains quantitative information about interfacial layers as well as ferroelectrically passive zones in the bulk. The derived interfacial capacitance is smaller than that estimated from conventional extrapolation techniques. In addition, the concept of depolarization is used for the investigation of fatigue behavior of PZT thin films indicating that the mechanism of seed inhibition, which is responsible for the effect, occurs in the entire film. *Published by AIP Publishing*. [http://dx.doi.org/10.1063/1.4992812]

INTRODUCTION

The effects of point defects in ferroelectric ceramics on the physical properties manifested in the hysteresis curve were analyzed by Arlt and co-workers in their electrostatic two-phase bulk model.[1] Beside the ferroelectric phase, the model consists of a non-ferroelectric phase due to the presence of defects which may be polar or nonpolar. By definition, even the polar defect species do not switch under an external electrical field. The authors could trace the shearing of the hysteresis curve to all kinds of defects, whereas the shifting of the loop along the field axis is caused by oriented polar defects often referred to as internal bias.[2] The variation of the coercive field strength is provoked by the inhomogeneous dielectric behavior. Two scenarios of a two-phase system were considered in Ref. 1: (i) two layers of a ferroelectric as well as a non-ferroelectric region with polar defects, and (ii) spherical inclusions of non-ferroelectric defects in a surrounding ferroelectric matrix. Assuming that the polarization P_2 and the relative permittivity ε_2 of the ferroelectric differs from P_1 and ε_1 of the non-ferroelectric polar phase (see Fig. 1), the field in the ferroelectric phase E_2 for an external field E_0 is given by

$$E_2 = \kappa E_0 + E_N + E_{ib}. \tag{1}$$

The first term represents a rescaling of the field axis by a factor $\kappa = 1 - c(\varepsilon_2 - \varepsilon_1)/B$. c is the volume fraction of the non-ferroelectric phase, i.e., the defect concentration. B is a dielectric coefficient which depends on the above mentioned scenarios: (i) two layers: $B_\ell = \varepsilon_1 - c(\varepsilon_2 - \varepsilon_1)$ and (ii) spherical inclusions: $B_{SI} = 2\varepsilon_2 + \varepsilon_1 - c(\varepsilon_2 - \varepsilon_1)$. E_N stands for the depolarization field leading to a slanting of the hysteresis loop

$$E_N = -N\frac{P_2}{\varepsilon_0} \quad \text{with } N = \frac{c}{\varepsilon_0 B}, \tag{2}$$

the size of which is given by the depolarization factor N. This behavior may be better known in magnetic materials.[3] The last term is known as the internal bias field E_{ib}

$$E_{ib} = M\frac{P_1}{\varepsilon_0} \quad \text{with } M = \frac{\Delta c}{\varepsilon_0 B} \tag{3}$$

containing P_1 and causes a shift of the $P(E)$ curve along the field axis. It is obvious that for nonpolar defects ($P_1 = 0$) this field vanishes. Δc represents the difference between the number of polar defects which are aligned in the direction of the surrounding ferroelectric polarization P_2 and those which are opposite oriented.[4] Taking into account that the alignment of the defect dipoles, and therefore the increase in the net-oriented part of defects, is a time-dependent, thermal activated process stabilizing the polarization orientation of each domain, the concept of the internal bias field can be used to describe the aging effect, i.e., the imprint, of ferroelectric materials. In that case, the internal bias field becomes a time-dependent function $E_{ib}(t) = \Delta c(t)P_1/\varepsilon_0 B$. A detailed derivation of this time-dependence in $BaTiO_3$ ceramics is given in Refs. 5 and 6.

The objective of this contribution is the extension of the two-phase model to a more complex phase system in order to describe the situation in real (non-defect-free) ferroelectric thin films containing an interfacial or dead layer between the electrode and the ferroelectric itself. These passive layers are believed to have permittivity significantly below the value of the bulk. There are various possible explanations of this effect, ranging from a finite electrostatic screening length in the electrode over growth induced defects and strain effects to effects of the electrode material.[7–12] In addition, the ferroelectric

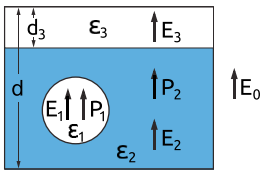

FIG. 1. Scheme of a non-ferroelectric polar spherical inclusion, representing a defect cell (subscript 1), in a homogeneous ferroelectric matrix (subscript 2) in the presence of a non-ferroelectric interface layer (subscript 3) between the ferroelectric and the electrode under an applied external field E_0.

[a]boettger@iwe.rwth-aachen.de. URL: www.emrl.de

polarization fatigue, which was extensively investigated due to fundamental physical aspects as well as due to reliability issues for devices,[13–15] is included into the depolarization concept in a phenomenological way. The aim, at least, is to show that the detailed analysis of conventional hysteresis loops has the potential for a semi-quantitative description of the interface layer and the fatigue effect which may lead to a deeper understanding of the behavior of ferroelectric thin films.

THE DEPOLARIZATION FACTOR

Starting point of the considerations is the combination of the two scenarios of a non-ferroelectric defect layer and inclusions of non-ferroelectric defects of the Arlt's model to a three-phase system, as shown in Fig. 1. This approach reflects the situation in a real (non-defect-free) ferroelectric thin film in the presence of an interfacial or dead layer. It is assumed that the dead layer between the electrode and the ferroelectric itself consists of non-polar defects while polar defect dipoles exist in the ferroelectric bulk.

The calculation of the field inside the ferroelectric E_2 can be easily derived from Eq. (1) by superposition in the way that field E_2 of scenario (i) is set as E_0 of scenario (ii). Neglecting the rescaling effect of the field axis and low defect concentrations $c \ll 1$ leads to $\kappa = 1$ and $B = 2\varepsilon_2 + \varepsilon_1$ as well as to a modified depolarization factor

$$N = \frac{d_3}{\varepsilon_3}\frac{1}{d} + \frac{c}{2\varepsilon_2 + \varepsilon_1}, \tag{4}$$

where d is the total thickness of the film, d_3 is the thickness of the interface layer, and ε_3 describes its dielectric permittivity. As in the two-phase system, the properties and the alignment over time of the defect dipoles determine the internal bias field. The depolarization field, however, is caused by bulk defects as well as the interface layer. Assuming a constant thickness of the dead layer at fixed dielectric properties, N scales linearly to the reciprocal film thickness with an offset related to the defect concentration. It is crucial that the dead layer thickness, as well as the defect concentration, is independent of the total film thickness. Similarly, the separation of the depolarization factor, following Eq. (4), becomes possible. To fulfill the requirements, the number and/or size of the inclusions has to be sufficiently low and the film thickness has to be large enough. The inclusions consist of single lattice cells or accumulations of few cells which contain point defects. Even in case of accumulations, the dimensions of an inclusion are estimated to be in the order of 1–2 nm. For ultra-thin films below 20 nm, this might play a decisive role. For the investigated and discussed thickness range larger than 90 nm, we exclude an impact.

It is possible to determine the depolarization factor from measured hysteresis loops $P_2(E_0)$. The basic assumption is that in a pure ferroelectric without any second phases, i.e., without any depolarization effect, the slope of the "intrinsic" hysteresis $P_2(E_2)$ at $E = E_C$ is infinite. Each depolarization leads to a slanting of the hysteresis loop. The transition from $P_2(E_2)$ to $P_2(E_0)$ corresponds to a shearing of the hysteresis and the opposite transition to a back-shearing, which are illustrated in Fig. 2. Therefore, the back-shearing procedure

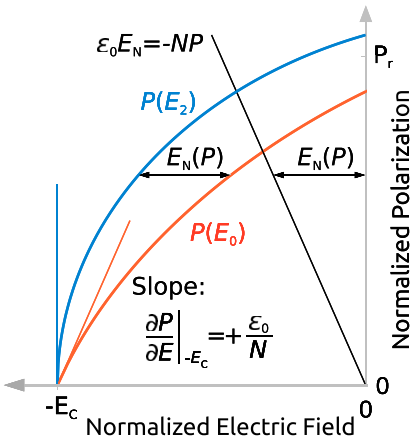

FIG. 2. Second quadrant of the hysteresis loop describing the depolarization effect with the material-specific polarization behavior as a function of the electric field in the ferroelectric $P(E_2)$ (blue curve) and the measured polarization as a function of the external field $P(E_0)$ (red curve). The conversion between $P(E_2)$ and $P(E_0)$ is given by the shearing line (black line) which allocates each P-value to the corresponding depolarization field E_N. As a result, the slope of the "sheared" hysteresis at the coercive field E_C is inversely proportional to the depolarization factor N. In case of no depolarization, as for $P(E_2)$, $N = 0$.

of a measured hysteresis loop provides information about the depolarization factor which directly results from the differentiation of Eq. (1)

$$\left.\frac{\partial E_2}{\partial P_2}\right|_{E_2=E_C} = \left.\frac{\partial E_0}{\partial P_2}\right|_{E_2=E_C} - \frac{N}{\varepsilon_0} \equiv 0, \tag{5}$$

with $\partial P_2/\partial E_0 = +\varepsilon_0/N$ in a narrow range around the coercive field. The effect of depolarization on the tilt of a perfectly square loop of the ferroelectric layer by a passive interface layer has already been discussed elsewhere.[15,16]

The presented approach is applied to estimate quantitatively the interface capacitance from large-signal hysteresis curves. The plot of $N(1/d)$ for a thickness series of ferroelectric thin films will result in a linear function whose slope corresponds to the ratio of the thickness and the permittivity of the interface $d_3/\varepsilon_0\varepsilon_3$, and therefore to the reciprocal area capacitance A/C_i. Additional information about defect bulk concentration c and the dielectric permittivities ε_1, ε_2 is given by the $N(1/d)$-axis intercept.

This is a different technique to the established method of extrapolating the reciprocal area capacitance A/C, measured by the small signal $C(V)$-curves, on the film thickness scale down to $d = 0$.[7,17,18] Since the interface and the bulk are considered as a capacitor divider, the y-axis intercept of the $A/C(d)$-plot matches the ratio $A/C_i = d_3/\varepsilon_0\varepsilon_3$

$$\frac{A}{C} = \frac{\varepsilon_2 - \varepsilon_3}{\varepsilon_2}\frac{d_3}{\varepsilon_0\varepsilon_3} + \frac{d}{\varepsilon_0\varepsilon_2} \approx \frac{A}{C_i} + \frac{d}{\varepsilon_0\varepsilon_2}. \tag{6}$$

It is essential that the properties as well as the thickness of the interface layer do not scale with the film thickness.

EXPERIMENTAL

PZT (lead zirconate titanate) films with a composition of 30/70 as well as 52/48 were deposited by a 2-

butoxyethanol based sol-gel spin coating on standard commercial platinized Si-wafers ($Si/SiO_2/TiO_2/Pt$ (100 nm)). The butoxyethanol based precursor solution was synthesized by a modified technique described in Refs. 19 and 20. After each layer deposition, the films were pyrolized at 200 °C and 400 °C in air for 2 min each. The number of deposition and pyrolysis cycles determines the film thickness. For PZT 30/70, a thickness series between 90 and 300 nm was fabricated, and for PZT 52/48, a thickness range $70\,\text{nm} \le d \le 700\,\text{nm}$ was covered. After depositing the last layer, the final crystallization was performed at 700 °C in O_2 with a rapid thermal annealing step. Pt top electrodes of 100 nm were sputtered at RT and structured with a photolithography and lift-off process. A post-anneal to recover the sputter-induced damages was performed at 700 °C in O_2.

The electrical hysteresis loops $P(V)$ were monitored by an aixACCT TF 2000 analyzer system at 1 kHz. For the capacitance measurements $C(V)$, a LCR-bridge hp 4284A with an AC signal (50 mV at 1 kHz) was used sweeping the bias field with 0.1 Hz. The fatigue cycling was performed with rectangular pulses of 100 kHz while the hysteresis measurement was equidistantly recorded on a logarithmic time scale.

INTERFACE CAPACITANCE

The depolarization factors of a thickness series of PZT 30/70 thin films were determined from large signal hysteresis measurements and plotted as a function of the inverse film thickness $N(1000/d)$ (see Fig. 3). The slope of the resulting straight line corresponds to the ratio $d_3/\varepsilon_3 = 0.004$ nm, which is equivalent to an inverse interface capacitance per area of $A/C_i \approx 0.5$ m^2/F or 0.0005 μm^2/fF. The y-axis is intercepted at $N_0 = 0.3 \times 10^{-5}$ which fits to a defect concentration $c \approx 0.5\%$ since the dielectric constants for the defect and the ferroelectric region are set to $\varepsilon_1 = 300$ and $\varepsilon_2 = 600$. The latter value is reasonable for the PZT material far away from the morphotropic phase boundary, and the first one may be regarded as an upper limit for non-ferroelectric perovskites, as it is observed for $SrTiO_3$ bulk ceramics.[21] The defect concentration thus determined is typical for a natural (often acceptor-like) contamination of undoped chemical solution deposition (CSD)-prepared films.

To compare these results with those from the conventional method by the means of small signal $C(V)$ measurements, the inverse area capacitance A/C is plotted in Fig. 4. The line fit leads to a slope of $\Delta(A/C)/\Delta d \approx 0.2 \times 10^9$ m/F matching very well the dielectric coefficient of the ferroelectric $\varepsilon_2 = 600$ used in the depolarization approach mentioned earlier. The estimated intercept in Fig. 4 represents an inverse interface capacitance $A/C_i \approx 4$ m^2/F which is in the same order of magnitude found for ferroelectric films by other authors, e.g., Ref. 22, using the same extrapolation procedure.

However, this value is 8 times larger than the value of the previously suggested technique. It is highly likely that the dielectric non-linear behavior of ferroelectrics is playing a non-negligible role since the film thickness is scaled down. In that case, the film thickness may vary the actual ac field strength when a constant voltage amplitude is applied leading to a modified dielectric response.[23] A second origin of the difference may rise from different sweep frequencies of $C(V)$ at 0.1 Hz and $P(V)$ at 1 kHz. Bolten *et al.* have investigated the frequency dependence of the coercive field as well as the maximal capacitance values. The effects are especially high for ferroelectric strontium bismuth tantalate (SBT) films, yet also observable in PZT films.[24,25] An analysis of already published hysteresis data[26] indicates an enhanced slanting of the loop, i.e., an enlargement of the depolarization effect, with increasing measuring frequency.

Finally, the thickness of the interface layer d_3 is estimated using again the above suggested value of $\varepsilon_3 = 300$ for the non-ferroelectric regions. The depolarization method leads to $d_3 \approx 1.2$ nm which is equivalent to three unit cells,

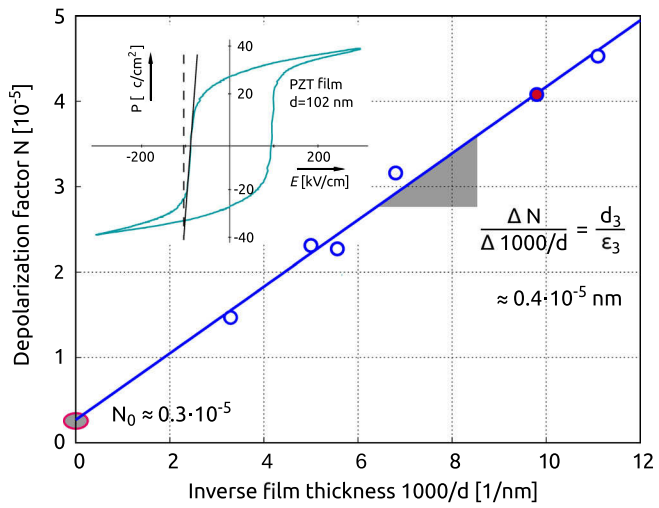

FIG. 3. Depolarization factor as a linear function of the inverse total film thickness of different PTZ 30/70 with a slope of $\Delta N/\Delta 1000/d \approx 0.4 \times 10^{-5}$ nm and a y-axis intercept $N_0 \approx 0.3 \times 10^{-5}$ for thicknesses $90\,\text{nm} \le d \le 304\,\text{nm}$. The inlet exemplarily shows the $P(E)$ loop from the measured $P(V)$ hysteresis and the estimated slope of $\partial P/\partial E$ at E_C for a thickness $d = 102$ nm. The corresponding depolarization factor is illustrated by the red-filled circle.

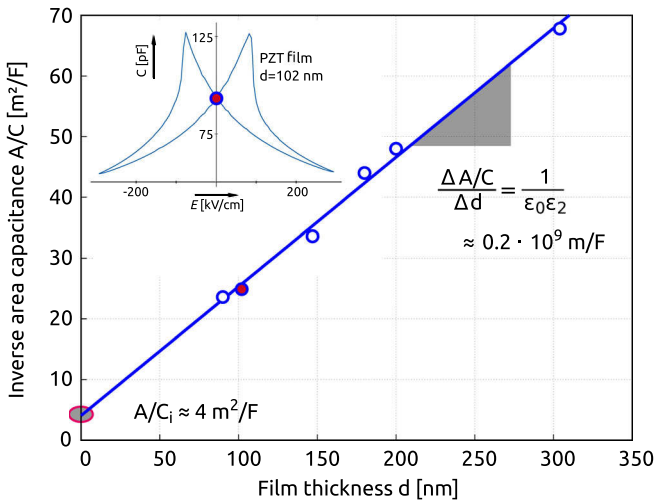

FIG. 4. Inverse area capacitance as a linear plot of PTZ 30/70 for a series of film thicknesses in the range $90\,\text{nm} \le d \le 304$ nm (blue line). The points result from measured $C(V)$ curves at zero voltage as shown exemplarily in the inlet of thickness $d = 102$ nm. The measured capacitance of $C \approx 95$ pF corresponds to an "effective" relative dielectric permittivity $\varepsilon \approx 440$ since $A = (50\,\mu\text{m})^2$. The linear fit for all thicknesses leads to a line with a slope of $\Delta A/C/\Delta d \approx 0.2 \times 10^9$ m/F which is related to the dielectric bulk behavior and a y-axis intercept $A/C_i \approx 4$ m^2/F which is the inverse area interface capacitance.

the A/C-extrapolation results in $d_3 \approx 10\,\text{nm}$ (25 unit cells). It is assumed that the latter method suffers from a higher amount of uncertainty for primarily two reasons: the mentioned dielectric non-linearity and the fact that the determination of the slope of a line in an accessible thickness range is much more precise than the extrapolation to a film thickness of $d = 0$.

FATIGUE EFFECT

The concept of depolarization is applied to describe the fatigue effect in ferroelectric thin films. Fatigue was discussed in the framework of pinning,[27,28] local imprint,[29] and enlargement of the interface layer,[30] which may be linked to the formation of a Pb/Pt phase[31] or a decrease of the effective capacitor area.[32] By investigating the unipolar and purely DC fatigue driven shifts in the polarization and piezoelectric hysteresis as well as asymmetries in the strain, Balke *et al.* proposed a charge carrier drift under the depolarizing field, and/or charge injection. Both mechanisms can mostly explain the effects they observed.[33] For fatigue behavior under bipolar electrical cycling, a damaged microstructure close to the electrodes was found. The fatigue behavior can be mainly attributed to these damaged areas.[28,34]

The dominant mechanism we suggested is a charge injection of electronic carriers from the electrode into nearby-electrode regions and a subsequent suppression of opposite domain nucleation, so-called seed inhibition.[12,35] In a more detailed picture, during polarization reversal of a domain, the polarization oriented along the external electrical field grows in the direction of the opposite electrode starting from a seed.[36] By expansion of this domain, a front of non-screened polarization charges (div $\mathbf{P} \neq 0$) propagates. This front locally evokes a high field strength leading to an injection of electronic charge carriers into the film. The injected charge blocks the complete reversal of the domain and prevents further reversal processes. This also happens with repeated reverses of the external field. Each reversal enhances the probability that the domains will be clamped by the injected charges. The amount of injected charge depends on the injection current density and the effective reversal time. In the framework of this approach, the impact of electrode materials on fatigue can be understood. Materials with lower work functions than that of Pt reduce the barrier of the metal-semiconductor transition and enhance the probability that trapped electronic carriers are released again since the field is reversed. Especially the use of oxide electrodes improves the fatigue behavior.[37] IrO_x (Ref. 36) as well as $SrRuO_3$ (Ref. 38) have lower work functions than Pt and avoid/reduce fatigue effects. Same results are also found for Cu bottom electrodes.[39] It is obvious that oxide electrodes with low work functions on one side are sufficient for fatigue prevention in order to facilitate a de-trapping of the captured charge.

In principle, ionic charge carriers due to the exchange of oxygen through the Pt electrode,[40] may also contribute to the seed inhibition process.

In Fig. 5, the fatigue results of a series of hysteresis measurements of PZT 52/48 capacitors with a film thickness of 121 nm are illustrated. The normalized remanent

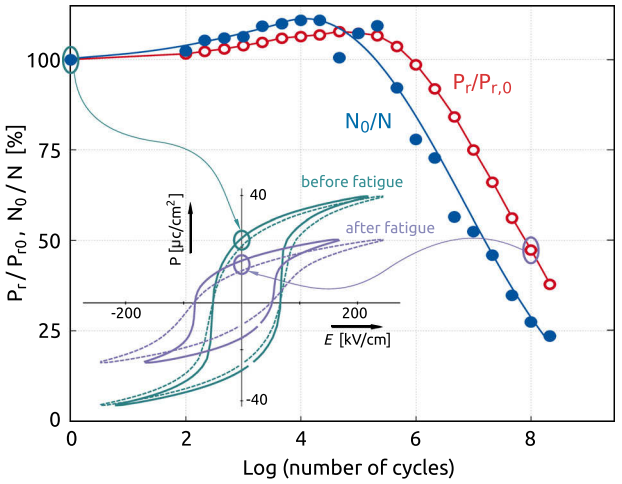

FIG. 5. Normalized remanent polarization $P_r/P_{r,0}$ (red) as well as normalized inverse depolarization factor N_0/N (blue) as a function of different fatigue states for a PZT 52/48 thin film with a thickness of 121 nm. The inlet exemplarily shows the measured hysteresis curves before fatigue (dotted green curve) and after 10^8 cycles (dotted violet curve). The back-sheared $P(E)$ loops are indicated by the full lines.

polarization $P_r/P_{r,0}$, as a function of the logarithmic number of switching cycles, shows after an initial wake-up process which is characteristic for various ferroelectric thin films.[41] Simultaneously, the depolarization is enlarged becoming evident by the reduction of the normalized inverse depolarization factor N_0/N. The values for N are taken from the back-shearing procedure of the hysteresis loops at each fatigue state as indicated by the inset of Fig. 5.

In a further step, a thickness PZT 52/48 film series in the range of $68\,\text{nm} \leq d \leq 708\,\text{nm}$ was investigated after different number of switching cycles in order to specify the influence of depolarization. As expected from Eq. (4), each fatigue state results in a straight line when the estimated depolarization factor N is plotted against the inverse film thickness (Fig. 6). Two clear trends are observed with the ongoing fatigue: the enlargement of the slope as well as the increase of the y-axis intercept. The first behavior is linked to a growth of the interface layer $d_3 = \varepsilon_3 \Delta N/\Delta(1000/d)$ as long as ε_3 is kept constant during the fatigue. The interpretation of the second observation needs a broadening of the term defect concentration c. In the beginning of this article it was introduced as the initial (process-controlled) desired and/or undesired defect concentration representing homogeneously distributed regions with non-ferroelectric properties in the matrix of the bulk ferroelectric. Now, the regions, which suffer from the above mentioned suppression of opposite domain nucleation (seed inhibition) and lose their ferroelectric characteristics during fatigue, are attributed to the "defect concentration" c. Therefore, the fatigue-related enlargement of $c = N_0(2\varepsilon_2 + \varepsilon_1)$ is due to the overall increase of non-ferroelectric bulk regions.

Since the dielectric coefficients are fatigue-independent ($\varepsilon_{1,3} = 300$ and $\varepsilon_2 = 600$), the temporal development of interface thickness and the part of non-ferroelectric bulk regions for thin films of PZT 52/48 are calculated using Eq. (4), see Table I. When the polarization is reduced by half $\Delta P_r(n)/$

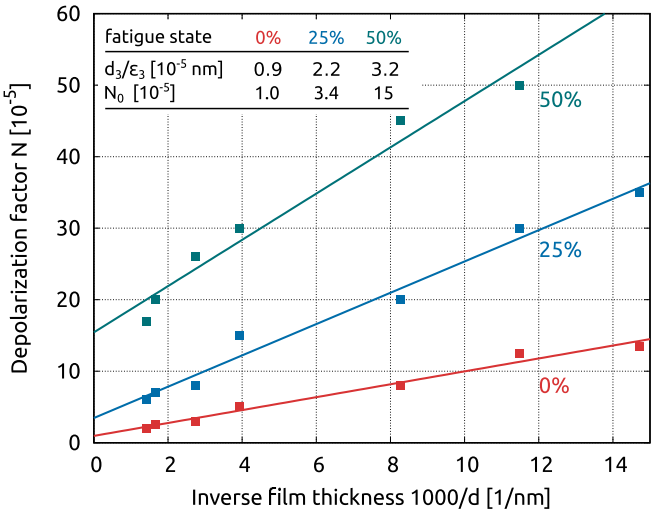

FIG. 6. Depolarization factor as a linear function of the inverse total film thickness of different PTZ 52/48 for thicknesses 68 nm $\leq d \leq$ 708 nm at different fatigue states: before fatigue (0%), after 10^6 cycles (25%), and after 10^7 cycles (50%). The ongoing fatigue corresponds to an enlargement of the slope $\Delta N/\Delta 1000/d = d_3/\varepsilon_3$ as well as with an increase of the y-axis intercept N_0.

TABLE I. Decrease of normalized remanent polarization $\Delta P_r(n)/P_r(1)$, interface thickness d_3, and concentration of non-ferroelectric bulk regions c depending on the number of cycles of electrical loads for PZT 52/48 films.

Number of cycles n	1	10^7	10^8
Fatigue state $\Delta P_r(n)/P_r(1)$	0%	25%	50%
Interface thickness d_3 (nm)	3	6.5	10
Non-ferroelectric bulk regions c	0.01	0.05	0.23

$P_r(1) = 50\%$ with $\Delta P_r(n) = P_r(1) - P_r(n)$, the thickness of the interface is approximately expanded from 3 nm to 10 nm. Concurrently, the proportion of non-ferroelectric bulk regions grows from 1% to 23% after 10^8 cycles. Based on this analysis, it is highly probable that the seed inhibition responsible for the fatigue mechanism takes place in the bulk as well as at the interface between the bulk and electrode.

CONCLUSIONS

Depolarization effects rise from interfacial layers and non-ferroelectric inclusions in the bulk modifying the shape of large-signal hysteresis loop of ferroelectric thin films. The degree of depolarization can be determined from the tilt of hysteresis curves. Under the assumption that the interface capacitance does not scale with the total film thickness, the depolarization factor is composed of a part which is dependent on the film thickness and into a constant one. Both the parts can be separated if a thickness series of thin films is analyzed, providing information about the interface layer and the defect concentration in the bulk. Compared with the conventional extrapolation method to estimate the interfacial capacitance of PZT thin films, the presented technique results in smaller values of A/C_i, however, it is considered to be more meaningful due to the prevention from dielectric non-linearities and due to the avoidance of extrapolation.

The concept of depolarization is applied to the investigation of fatigue. It could be shown for a thickness series of PZT thin films that not only suppression of opposite domain nucleation takes place in the regions nearby the interface layer but also seed inhibition is probable in the bulk. The creation of "ferroelectrically dead areas" appears along the entire film.

ACKNOWLEDGMENTS

This work was funded by the German Research Foundation (Deutsche Forschungsgemeinschaft) within the scope of the project "FeCaps" (Project No. WA 908/18).

[1]U. Robels, J. H. Calderwood, and G. Arlt, J. Appl. Phys. **77**, 4002 (1995).
[2]H. Neumann and G. Arlt, Ferroelectrics **76**, 303 (1987).
[3]J. D. Jackson, *Classical Electrodynamics*, 2nd ed. (John Wiley & Sons, 1975).
[4]K. Carl and K. H. Hardtl, Ferroelectrics **17**, 473 (1977).
[5]G. Arlt and H. Neumann, Ferroelectrics **87**, 109 (1988).
[6]R. Lohkamper, H. Neumann, and G. Arlt, J. Appl. Phys. **68**, 4220 (1990).
[7]R. Plonka, R. Dittmann, N. A. Pertsev, E. Vasco, and R. Waser, Appl. Phys. Lett. **86**, 202908 (2005).
[8]J. Im, S. K. Streiffer, O. Auciello, and A. R. Krauss, Appl. Phys. Lett. **77**, 2593 (2000).
[9]H. C. Li, W. D. Si, A. D. West, and X. X. Xi, Appl. Phys. Lett. **73**, 464 (1998).
[10]C. T. Black and J. J. Welser, IEEE Trans. Electron Devices **46**, 776 (1999).
[11]M. Stengel, D. Vanderbilt, and N. A. Spaldin, Nat. Mater. **8**, 392 (2009).
[12]E. L. Colla, A. K. Tagantsev, D. V. Taylor, and A. L. Kholkin, Int. Ferroelectr. **18**, 19 (1997).
[13]C. A. de Araujo, J. D. Cuchiaro, L. McMillan, M. Scott, and J. Scott, Nature **374**, 627 (1995).
[14]P. J. Schorn, D. Brauhaus, U. Bottger, R. Waser, G. Beitel, N. Nagel, and R. Bruchhaus, J. Appl. Phys. **99**, 114104 (2006).
[15]D. Damjanovic, Rep. Prog. Phys. **61**, 1267–1324 (1998).
[16]A. K. Tagantsev, M. Landivar, E. Colla, and N. Setter, J. Appl. Phys. **78**, 2623 (1995).
[17]L. J. Sinnamon, R. M. Bowman, and J. M. Gregg, Appl. Phys. Lett. **78**, 1724 (2001).
[18]S. K. Streiffer, C. Basceri, C. B. Parker, S. E. Lash, and A. I. Kingon, J. Appl. Phys. **86**, 4565 (1999).
[19]K. D. Budd, S. K. Dey, and D. A. Payne, Br. Ceram. Proc. **36**, 107 (1985).
[20]T. Schneller and R. Waser, Ferroelectrics **267**, 293 (2002).
[21]B. K. Choudhuray, K. V. Rao, and N. P. Choudhuray, J. Mater. Sci. **24**, 3469–3474 (1989).
[22]J. J. Lee, C. L. Thio, and S. B. Desu, J. Appl. Phys. **78**, 5073 (1995).
[23]U. Ellerkmann, R. Liedtke, and R. Waser, Ferroelectrics **271**, 315 (2002).
[24]D. Bolten, O. Lohse, M. Grossmann, and R. Waser, Ferroelectrics **221**, 251 (1999).
[25]D. Bolten, U. Bottger, T. Schneller, M. Grossmann, O. Lohse, and R. Waser, Appl. Phys. Lett. **77**, 3830 (2000).
[26]D. Bolten, "Reversible and irreversible polarization processes in ferroelectric ceramics and thin films," Ph.D. thesis (RWTH Aachen, 2002).
[27]W. Warren, D. Dimos, G. Pike, K. Vanheusden, and R. Ramesh, Appl. Phys. Lett. **67**, 1689 (1995).
[28]Z. Luo, T. Granzow, J. Glaum, W. Jo, J. Rödel, and M. Hoffman, J. Am. Ceram. Soc. **94**, 3927 (2011).
[29]V. Shur, E. Nikolaeva, E. Shishkin, I. Baturin, D. Bolten, O. Lohse, and R. Waser, in *Ferroelectric Thin Films IX Symposium, Boston, MA, USA, 26/11/2000-30/11/2000* (Institute of Physics and Applied Mathematics, Ural State University, Ekaterinburg, Russia/Mater. Res. Soc. Symp., Warrendale, PA, USA, 2001), pp. CC10.8.1–CC16.
[30]P. K. Larsen, G. J. M. Dormans, D. J. Taylor, and P. J. van Veldhoven, J. Appl. Phys. **76**, 2405 (1994).
[31]Z. Huang, O. Zhang, and R. W. Whatmore, J. Mater. Sci. **17**, 1157 (1998).
[32]E. L. Colla, A. K. Tagantsev, D. Taylor, and A. L. Kholkin, J. Korean Phys. Soc. **32**, 1353 (1998).
[33]N. Balke, D. C. Lupascu, T. Granzow, and J. Rödel, J. Am. Ceram. Soc. **90**, 1081 (2007).

[34]N. Balke, H. Kungl, T. Granzow, D. C. Lupascu, M. J. Hoffmann, and J. Rödel, J. Am. Ceram. Soc. **90**, 3869 (2007).
[35]A. K. Tagantsev, I. Stolichnov, E. L. Colla, and N. Setter, J. Appl. Phys. **90**, 1387 (2001).
[36]D. Bräuhaus, "Fatigue und Imprint an ferroelektrischen Dünnschichten," Ph.D. thesis (RWTH Aachen, 2010).
[37]R. Ramesh *et al*., Appl. Phys. Lett. **61**, 1537 (1992).
[38]H. Miyazaki, Y. Miwa, and H. Suzuki, Mater. Sci. Eng. B **136**, 203 (2007).
[39]A. Kingon and S. Srinivasan, Nat. Mater. **4**, 233 (2005).
[40]K. Szot, W. Speier, G. Bihlmayer, and R. Waser, Nat. Mater. **5**, 312 (2006).
[41]T. Schenk, M. Hoffmann, J. Ocker, M. Pešic, T. Mikolajick, and U. Schroeder, ACS Appl. Mater. Interfaces **7**, 20224 (2015).